PROCESSING AND CHARACTERIZATION OF B_4C-SiC/(Al,Si) MULTI-CARBIDES COMPOSITES.

B. A. Almeida[a,*], A. Ravanan[a], M. C. Ferro[a], P. M. F. Grave[a], H-Y Wu[b], M-X Gao[b], Y. Pan[b], F. J. Oliveira[a], A. B. Lopes[a] and J. M. Vieira[a]

[a]*University of Aveiro, Dep. of Materials Engineering and Ceramics, CICECO - Centre for Research in Ceramics and Composite Materials, Campus Universitário de Santiago PT-3810-193 Aveiro, Portugal*
[b] *Zhejiang University, Department of Materials Science and Engineering & State Key Laboratory of Silicon Materials CN-310027 Hangzhou, P.R. China*

**brunoalmeida@ua.pt*

Keywords: B_4C, composites, mechanical properties, EBSD.

Abstract:
B_4C-SiC/(Al, Si) multi-carbide composites were obtained by reactive melt infiltration of B_4C with Al-Si binary alloy for short times. Phases were characterized by X-ray diffraction. The microstructure and spatial distribution of phases was assessed by SEM with EDS and EBSD. The mechanical properties of hardness and indentation fracture toughness were evaluated and compared with similar results recent published works of composites processed for longer times. The value of EBSD analysis to understand the role of interfaces and brittle/ ductile phases in crack growth resistance is further discussed.

1. Introduction

The low reliability of the hard, low density ceramics coming from the inherent limited fracture energy may be overcome by forming composites strengthened by stiff fibers or plastically yielding metallic inclusions that operate in the crack bridging zone [1-3]. Among the light weight engineering materials, the B_4C ceramics and composites have been extensively studied and find use in technology [4]. Poor sintering of B_4C demanding high temperatures (1700-2200 ºC) coupled to the use applied pressure as in hot-pressing and spark plasma sintering makes processing expensive [5-6]. Reactive infiltration of B_4C with low density Al-Si alloys was early demonstrated by Frage *et al* [7] and gave the possibility to prepare B_4C-based composites at moderate prices [4, 7-11].
The low density, large ductility of aluminum and wide availability at low price, make Al a relevant selection for strengthening the ceramic matrix. However, wetting of B_4C by molten Al is strongly dependent on temperature, being poor at temperatures below 1000 ºC although it can improve with selective additions of other metals [7, 12]. Precipitation of easy cleaving Al_4C_3 is harmful for the mechanical strength of theses composites [7, 12] whereas the presence of SiC increases the hardness and elastic modulus of the composites [5, 11, 13]. The spontaneous infiltration of porous B_4C with Al-Si alloys has been described already [4, 7, 14]. The objective of the work is to minimize infiltration time without compromising mechanical properties and preserving enough Si in the liquid to prevent formation of the brittle Al_4C_3 phase, the threshold composition being 12.6 wt% Si [15]. EBSD has been applied in the study

of crack growth to assess plastic deformation at the crack tip [3, 16]. This study aims to characterize the mechanical properties of hardness and indentation fracture toughness in relation to the phases of B_4C composites and to give further insight onto the operation toughening mechanisms in bridging zone near the crack tip of the Vickers indention flaw.

2. Experimental Procedure

Reactive infiltration of as-pressed cylindrical pellets of B_4C with 7.5 mm height was done in a graphite furnace with Ar atmosphere as described in reference [4, 14], for short dwell times (5 min) at maximum temperatures of infiltration, 1200-1300 ºC. A B_4C powder with average particle size of 10 µm was used. The Al-Si batches containing 25 and 35 wt. % Si were prepared by melting the alloys at 1000 ºC under Ar atmosphere. The density of the composites was obtained by Archimedes method. Crystalline phases were identified by X-ray diffraction (XRD), RIGAKU Geigerflex. To quantify phase fractions, a set of mixtures of the Al, Si, B_4C and SiC powders were analyzed by XRD. The ratio of intensities of the main XRD lines of the phases were used as calibration functions to establish the fraction of each crystalline phase in the Al-Si alloys and in the composites. Difficulties inherent to prepare of EBSD qualified samples of B_4C-Al and Al-Si melt infiltrated B_4C composites were recently described [14, 17]. The composite was mechanically polished using diamond lapping papers of 30, 15, 9, 6, 3, 1 and 0.5 µm particle sizes, followed by finishing with a colloidal silica suspension, Ted Pella, Inc., 0.06 µm particle sizes. The polished surfaces of the composites were lightly C coated. Samples were characterized by SEM, Hitachi SU-70, equipped with EDS spectroscopy, B-U Bruker Quantax 400, and diffraction (EBSD, Bruker CrystAlign QC 400). Vickers microhardness was measured with a Shimadzu Data Letty 150 a diamond pyramid at 1 kgf of applied load. Vickers hardness at loads of 10 and 30 kgf was determined with the Zwick/Roell ZHU tester. Vickers hardness, H_V, and indentation fracture toughness K_{IC} (Anstis equation) were calculated as [18, 19]:

$$H_V = 2\sin\left(\frac{136^\circ}{2}\right)\frac{P}{a^2} \tag{1}$$

$$K_{IC} = 0.016\sin\left(\frac{E}{H_V}\right)^{\frac{1}{2}}\frac{P}{c^{3/2}} \tag{2}$$

where E is the Young modulus, P the applied load, a the average length of the diagonal of the indenter impression and c the length of the median/radial crack.

3. Results and Discussion

Although residual carbon of B_4C powders may improve mechanical properties of the B_4C-C composites [20], there is also the risk that graphite in B_4C might reduce the strength of Al-Si melt infiltrated B_4C composites [4] so low graphite 10 µm B_4C powder was used. Two batches of the Al-Si containing 25 and 35 wt% Si were made. A third batch with 25 wt. % Si and melted twice was also prepared. Details of phase composition of the Al-Si determined by XRD, the microstructure and distribution of Si and Al crystalline phases determined by EBSD were given elsewhere [14]. XRD and EBSD results confirm that the Si phase fraction in batches 1 and 3 is close to the nominal value. Al_2O_3 contamination from oxidation during melting was found in batch 2. No alumina was detected inside the composites prepared by melt infiltration from batch 2. In the solidification of the Al-Si alloys, the Si phase precipitates first as primary dendrites, the Al solidifying at the eutectic point, 573 ºC. Hardness and ductility of the Al-Si alloy are dependent on Si content, dendrite size and the

distribution of the two phases which can be changed by adjusting the cooling conditions during solidification [21, 22].

3.1. B_4C-SiC/(Al-Si) composites.

The Al-Si melts used for infiltration the B_4C preforms yielding the three composites of this study were selected as follows: composite A (batch 1); composite B (batch 2) and composite C (batch 3). The three samples of the composites have high density with residual porosity below 1.5 %. Poor wetting from contaminants would decrease the direct contact between the Al-Si and the B_4C skeleton and would lead to irregular infiltration [23]. Besides freshly formed SiC, Al-B-C phases may also precipitate during the reactive melt infiltration of B_4C. Depending on experimental conditions several ternary phases of the Al-B-C system can form of which at least nine are reported in literature [24]. XRD spectra of the samples, sectioned along the cylindrical axis of pellets, are displayed in figure 1, revealing only four crystalline phases: Al, Si, B_4C and SiC. Traces of the Al_4C_3 and $Al_3B_{48}C_2$ were detected by XRD and SEM at the low-end of infiltration in the same cross-section of composite A [25]. The molar fractions of these four phases in the composites determined by the XRD analysis with standards and estimated by EBSD software are given in table 1.

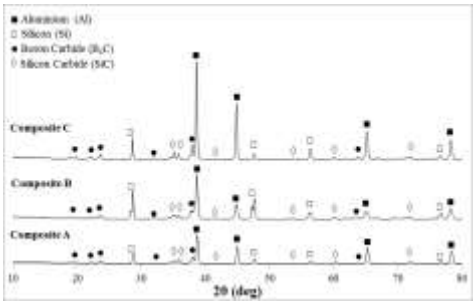

Figure 1: XRD results for three multi-carbide composites.

		Al	Si	B_4C	SiC	Zero solutions
XRD	Composite A	44,6	17,2	33,0	5,2	-
	Composite B	43,9	18,7	32,9	4,4	-
	Composite C	54,9	12,5	29,3	3,3	-
EBSD	Composite A	38,1	18,5	40,2	3,1	22,8
	Composite B	34,4	17,6	44,3	3,7	31,9
	Composite C	31,3	27,8	38,8	2,1	24,9

Table 1: Molar fraction of main crystalline phases determined from XRD and estimated by EBSD software.

Both techniques gave phase molar fractions with slight differences, especially for Al and B_4C, due to low XRD line intensities of B_4C. Surface finishing of the polished surfaces takes a key role on indexing and quantification by EBSD, especially in multi-phase materials [14]. Figure 2 presents the SEM image, EDS elemental map and EBSD phase distribution of a representative area of the microstructure of these composites.

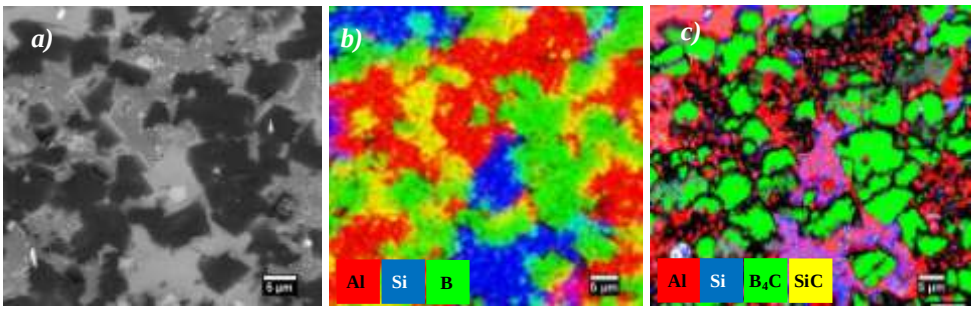

Figure 2: Multi-carbide B_4C-SiC/(Al,Si) composite C, a) SEM microstructure, b) elemental map from EDS; c) EBSD phase map for Al, Si, B_4C and SiC (0.115 µm step size).

The EDS map in Figure 2 b) of composite C gives the main features of the distribution of Al, Si and B in the composites and shows that the large metallic particles of light gray contrast in Figure 2 a) are Si dendrites. Of the same area, the crystalline phases presented on the EBSD map (figure 2 c)) show a phase distribution that closely follows the distribution of their constituting elements in the EDS map. Comparison of figures 2 b) and c) reveals that

simultaneous detection on B and Al by EDS (yellowed areas, Figure 2 b) is present at places where thin B_4C wedges overlap with Al grains underneath, this effect being explained by the deepness of the interaction volume for X-Ray emission in EDS. The crystalline lattices of both Al and Si phases have the same fcc (face-centered) cubic Bravais lattice with similar space groups [14], the Si dendrite material in Figure 2 c) being index in part to the Al phase by the EBSD algorithm of phase identification. This figure also displays a high proportion of black dots, named zero solutions, representing 23-32 % of not indexed solutions (table 1). They are observed at the hard particle edges and inside the Al showing slightly rougher surfaces. Passivation of Al can form an amorphous oxide layer with 2-4 nm thick [26] which adds to surface relief and smearing of the surface layer of Al originated from plastic deformation during polishing [17] and can explain poorer identification of the Al phase by EBSD. Final polishing with colloidal silica can either improve finishing of the surface or enhance relief differences between the grains of the hard and softer phases [14, 17].

3.2. Mechanical properties of the composites.

The following values of E and H_V, in GPa units, were obtained from literature for each of the phases of the composites in table 1: Al-69, Si-185, SiC-450 and B_4C-470 for the Young modulus [27-30] and 0.17 (Al), 9 (Si), 19 (SiC) and 28 (B_4C) for the hardness [31-34], respectively. Table 2 gives the values of E and H_V calculated by the rule of mixtures from the corresponding values of E and H_V of the solid phases and the volume fractions determined from the XRD results given in table 1. Values of H_V determined at three different applied loads, equation (1), and of K_{IC} determined for P = 98 N, equation (2), are also given in table 2.

Composite	**$E_{calc.}$ (GPa)**	**$H_{calc.}$ (GPa)**	**H_V (GPa)**			**ISE**		**K_{IC} ($MPa.m^{1/2}$)**
			9.8 N	**98 N**	**294 N**	**H_0 (GPa)**	**n**	
A	242	11.9	8.0 ± 3.0	5.8 ± 1.0	4.7 ± 0.2	11.5	1.73	7.5 ± 0.4
B	240	11.8	7.6 ± 2.0	5.9 ± 1.0	4.6 ± 0.1	10.7	1.75	8.3 ± 0.8
C	214	10.0	7.2 ± 2.0	6.4 ± 2.0	3.7 ± 0.4	11.5	1.70	7.6 ± 0.4

Table 2: Young modulus E, indentation hardness H_V and fracture toughness K_{IC} for the composites A, B and C.

Hardness and elastic modulus of composites increase with the amount of harder and stiffer phases. On this case, the ceramic-to-metal ratio strongly influences the calculated values of E and H_V. Accordingly, the decreasing of calculated values of E and H_V from composite A to C in table 3 results from composites A and B having higher content in B_4C+SiC phases than composite C, table 2. At the lowest and highest levels of P, composites A and B display higher experimental values of H_V than C, table 3. The opposite trend is observed at the intermediate value of P, the standard errors of H_V values being wide. H_V data of each composite in table 3 displays power law dependence on indentation load, P,

$$H_V = H_0 \, P^s \tag{3}$$

the exponent s being in the range -0.175 < s < -0.140, the values of H_0 being given in table 2. The values of H_0, the hardness of the material at P = 1 N, are close to the H_{calc} values. Such dependence of H_V on P is equivalent to the indentation size effect (ISE) given by Meyer´s law [35] which correlates P to the resulting indention dimension as,

$$P = C \, a^n \tag{4}$$

where C is a constant and the Meyer´s exponent is n = 2 for materials of constant hardness, equation (1), or otherwise n < 2 for materials displaying neat ISE dependence. The values Meyer´s exponent given in table 3 were calculated from s, as n = 2/(1-s). Reverse ISE

dependence, n > 2, had been observed in materials deforming predominantly by plastic yield [36, 37]. Values of n as low as 1.50-1.77 were early reported for hot-pressed Si_3N_4 based ceramics [38], n being dependent on residual porosity and grain size of the tested material. The observation of ISE in SiC, MgO and Al_2O_3 ceramics was correlated to elastic recovery at scales of the indentation imprint that approach spacing of the plastic deformation bands [39]. Microhardness testing of spark plasma sintered TiCN-Al_2O_3 cermets with Co-Ni metallic binder yielded slightly higher values of n in the range 1.77-1.83 rising with the content of metallic binder in the composite and coarsening of grain size [37]. The values of n in table 2 overlap with the range of values of n found in hard ceramics and cermets.

Figure 3 presents the EDS map an indentation crack and EBSD maps of the crack tip area. Indentation corners often do not nucleate the radial cracks in a straight way [4]. Particles close to the edges of the indenter imprint simply break in several directions, Figure 3 a). Concerning the determination of K_{IC}, only at indentation loads close to 98 N and above was it possible to follow the track of the radial cracks with the certainty enough for determination of K_{IC}. Analogous difficulties in determining the values K_{IC} of reactive melt infiltrate composites prepared with 36 wt% Si alloy at HV3 (29.4 N) were recently reported [9]. Values of K_{IC} in table 2 range from 7.5 up to 8.3 MPa.$m^{½}$. In spite of the scatter of K_{IC}, the high values of K_{IC} of the composites of the present study are correlated to the comparatively low values of H_V in the same way as observed in similar reactive melt infiltrated B_4C composites prepared with Al-Si alloys of higher Si content and longer reaction times [4].

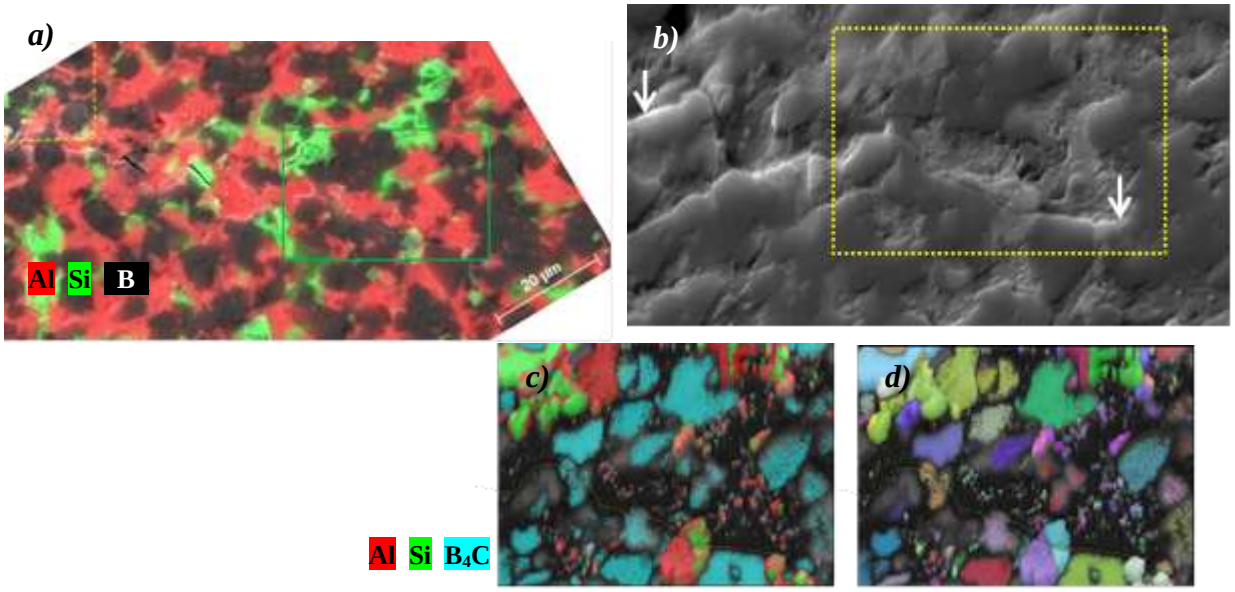

Figure 3: Multi-carbide B_4C-SiC/(Al,Si) composite C with 294 N indentation crack: a) EDS mapping of Al, Si overlaid on SEM microstructure with indentation marked on right (yellow) and region selected for EBSD (green); b) enlarged view of crack tip (arrow on right) and EBSD selected area (0.120 µm step size); c) Al, Si and B_4C phase mapping of EBSD; and d) orientation mapping by EBSD.

As in Figure 2 c), the EBSD phase map (Figure 3 c)) shows reliable indexing of the B_4C grains but with a lesser clear distinction between Al and Si grains of the metallic phase at some places. With the support of the EDS map, fragile fracture of Si particles occurred at three places along the crack, the last one being the small Si particle at the crack tip. The orientation map in Figure 3 d) shows a Si dendrite composed of two crystalline domains fractured by the advancing crack. In between these events the crack line (in yellow in figures 3 c) and 3 d)) followed the interface between hard B_4C particles and the plastically deformed Al grains. Crack deflection has a significant contribute to strengthening of the composite.

As in other studies of crack growth using EBSD, the plastic yield of the ductile phase in the crack bridging zone is revealed by intense slip and subgrain formation that rapidly increases the proportion of zero-solutions in EBSD maps [3, 16, 40, 41]. In comparison to the quality of Al indexing in Figure 2, the figures 3 c) and 3 d) revealed an elevated number of zero solutions not just at vicinity fracture line but also spreading into the area of the Al inclusions contacting the flaw. Plastic deformation of the Al inclusion is almost uniform in volume, the crack bridging by the soft metallic inclusions contributing at large to the work of fracture.

4. Conclusions

The study of the B_4C-based composites prepared by the reactive melt infiltration technique at temperatures between 1200 and 1300 ºC lead to the following conclusions:

- Successful infiltration of B_4C cylindrical preforms of 7.5 mm thickness had been achieved in short dwells of 5 minutes at the maximum temperature. The evaluation of the structural development and phase composition confirmed that besides the freshly formed SiC only the phases present in the raw materials are detected in the composites.
- Finishing of the polished surfaces with colloidal SiO_2 allowed reliable indexing of the B_4C phase by EBSD, but the amorphous layer formed on Al surface, relief or topography affected indexing in separate the Si and Al grains of the same fcc crystalline system.
- Vickers hardness of all three composites displays an indentation size effect that follows Meyer´s law with values of Meyer´s index of 1.70-1.75.
- EBSD analysis of the indentation flaws confirms crack deflection and mostly the nearly uniform yielding in the volume of the ductile Al ligaments in the crack bridging zone as the main contributes to the work fracture and corresponding large values of indentation fracture toughness K_{IC} of the composites of the present study.

Acknowledgements
The authors would like to acknowledge the RNME – Pole University of Aveiro (FCT Project REDE/1509/RME/2005) for access to SEM, scientific and technical assistance and one of the authors the EMMS consortium funded by the European Commission for the MSc scholarship.

References

[1] A. G. Evans. Perspective on the development of high-toughness ceramics. *Journal of the American Ceramic Society*, 73: 187-206, 1990.
[2] D. Munz. What can we learn from R-curve measurements? *Journal of the American Ceramic Society*, 90: 1-15, 2007.
[3] K.P. Mingard, H.G. Jones, M.G. Gee, B. Roebuck, J.W. Nunn. In situ observation of crack growth in a WC-Co hardmetal and characterization of crack growth morphologies by EBSD. *International Journal of Refractory Metals and Hard Materials*, 36: 136–142, 2013.
[4] H. Wu, S. Zhang, M. Gao, D. Zhu, Y. Pan, Y. Liu, H. Pan, F. J. Oliveira and J. M. Vieira. Microstructure and mechanical properties of multi-carbides/(Al, Si) composites derived from porous B_4C preforms by reactive melt infiltration. *Materials Science and Engineering A*, 551: 200-08, 2012.
[5] A. Li, Y. Zhen, Q. Yin, L. Ma and Y. Yin. Microstructure and properties of (SiC, TiB_2)/B_4C composites by reaction hot pressing. *Ceramics International*, 32: 849-56, 2006.

[6] A. Goldstein, Y. Geffen and A. Goldenberg. Boron Carbide-Zirconium Boride *In Situ* Composites by the Reactive Pressureless Sintering of Boron Carbide-Zirconia Mixtures. *Journal of the American Ceramic Society*, 84(3), 642-44, 2001.

[7] N. Frage, L. Levin, N. Frumin, M. Gelbstein and M. P. Dariel. Manufacturing B_4C-(Al,Si) composite materials by metal alloy infiltration. *Journal of Materials Processing Technology*, 143-144: 486-490, 2003.

[8] I. Mizrahi, A. Raviv, H. Dilman, M. Aizenshtein, M. P. Dariel and N. Frage. The effect of Fe addition on processing and mechanical properties of reaction infiltrated boron carbide-based composites. *Journal of Materials Science*, 42: 6923-28, 2007.

[9] S. Hayun, D. Rittel, N. Frage and M. P. Dariel. Static and dynamic mechanical properties of infiltrated B_4C-Si composites. *Materials Science and Engineering A*, 487: 405-409, 2008.

[10] S. Hayun, A. Weizman, M. P. Dariel, N. Frage. Microstructural evolution during the infiltration of boron carbide with molten silicon. *Journal of the European Ceramic Society*, 30: 1007-14, 2010.

[11] S. Hayun, N. Frage and M. P. Dariel. The morphology of ceramic phases in B_xC-SiC-Si infiltrated composites. *Journal of Solid State Chemistry*, 179: 2875-79, 2006.

[12] Q. Lin, P. Shen, F. Qiu, D. Zhang and Q. Jiang. Wetting of polycrystalline B4C by molten Al at 1173-1473 K. *Scripta Materialia*, 60: 960-963, 2009.

[13] D. Mallick, T. K. Kayal, J. Ghosh, O. P. Chakrabarti, S. Biswas and H. S. Maiti. Development of multiphase B-Si-C ceramic composite by reaction sintering. *Ceramics International*, 35: 1667-1669, 2009.

[14] B. A. Almeida, M. C. Ferro, A. Ravanan, P. M. F. Grave, H-Y. Wu, M-X. Gao, Y. Pan, F. J. Oliveira, A. B. Lopes and J. M. Vieira. Study of multi-carbide B4C-SiC/(Al, Si) reaction infiltrated composites by SEM with EBSD. *IOP Conference Series: Materials Science and Engineering*, 55: 012001, 2014

[15] J. C. Viala, P. Fortier, J. Bouix, Stable and metastable phase equilibria in the chemical interaction between aluminium and silicon carbide. *Journal of Material Science*, 25: 1842 -1850, 1990.

[16] H. Jin, W.Y. Lu, S. Haldar and H. A. Bruck, Microscale characterization of granular deformation near a crack tip. *Journal of Materials Science*, 46: 6596-6602, 2011.

[17] J. Guo, S. Amira, P. Gougeon and X.-G. Chen. Effect of the surface preparation techniques on the EBSD analysis of a friction stir welded AA1100-B4C metal matrix composite. *Materials Characterization*, 62: 865-877, 2011.

[18] R. L. S. G. E. Sandland. An accurate method of determining the hardness of metals, with particular reference to those of high degree of hardness. *Proceedings of the Institution of Mechanical Engineers*, vol. I, IMechE., 623-641, London, 1922.

[19] G. R. Anstis, B. R. Lwan and D. B. Marshall. A critical evaluation of indentation techniques for measuring fracture toughness: II, Strength method. *Journal of the American Ceramic Society*, 64(9): 533-38, 1981.

[20] K. A. Schwetz, L. S. Sigl and L. Pfau. Mechanical properties of injection molded B_4C-C Ceramics. *Journal of Solid State Chemistry*, 133: 68-76, 1997.

[21] L. N. Burminskaya, V. V. Zaboleev-Zotov, Y. M. Likulin and P. O. Pashkov. Strength of two-phase aluminum-base mixtures. Translated from *Metallovedenie I Termicheskaya Obrabotka Metallov*, 6: 27-30, 1967.

[22] V. Vijeesh and K. N. Prabhu. Review of Microstructure Evolution in Hypereutectic Al–Si Alloys and its Effect on Wear Properties. *Transactions of Indian Institute of Metals*, 67(1): 1-18, 2014.

[23] H. Ribes., R. Dasilva, M. Suéry and T. Bretheau, Effect of interfacial oxide layer in Al-SiC particle composites on bond strength and mechanical behavior. *Material Science Technology*, 6: 621–628, 1990.
[24] D. C. Halverson, A. J. Pyzik, I. A. Aksay and W. E. Snowden. Processing of Boron Carbide – Aluminum Composites. *Journal of the American Ceramic Society*, 72 [5]: 775-80, 1989.
[25] A. Ravanan. Processing and Toughening of Dual-Metallic Phase Dual-Carbide Composites. *EMMS Master Dissertation, University of Aveiro (PT)*, 2013.
[26] N. Eisenreich, H. Fietzek, M. M. Juez-Lorenzo, V. Kolarik, A. Koleczko and V. Weiser. On the Mechanism of Low Temperature Oxidation for Aluminum Particles down to the Nano-Scale. *Propellants, Explosives, Pyrotechnics*, 29 (3): 137-145, 2004.
[27] K. A. Schwetz, Silicon carbide based hard materials. Ed. R. Reidel, *Handbook of ceramic hard materials*, WILEY-VCH GmpH, Weinheim, 2000.
[28] William D. Callister, Jr. *Materials Science and Engineering*. John Wiley & Sons, Inc., New York, 2007. ISBN:978-0-471-73696-7.
[29] *MEMS - Fundamental, Technology and Applications*. CRC Press Taylor & Francis Group, LLC., Boca Raton, 2013. ISBN: 978-1-4665-1581-9.
[30] S. Hayun, V. Paris, M.P. Dariel, N. Frage, E. Zaretzky. Static and dynamic mechanical properties of boron carbide processed by spark plasma sintering. *Journal of the European Ceramic Society*, 29: 3395-3400, 2009.
[31] R. Telle, L. S. Sigl and K. Takagi. Boride-based hard materials. Ed. R. Reidel, *Handbook of ceramic hard materials*, WILEY-VCH, Weinheim, 2000.
[32] M. Gupta, S. Ling. Microstructure and mechanical properties of hypo/ hyper-eutectic Al–Si alloys synthesized using a near-net shape forming technique. *Journal of Alloys and Compounds*, 287: 287 – 294, 1999.
[33] J. Rey, G.M., Ph. Kapsa and J. L . Loubet, Boron carbide coatings : correlation between mechanical properties and LPCVD parameters values. *Journal De Physique*, 5: 311-321, 1989.
[34] X.J. Zhao, N. Zhang, H.Q. Ru, B. Liang, D.L. Chen. Mechanical properties and toughening mechanisms of silicon carbide nano-particulate reinforced Alon composites. Materials Science and Engineering A, 538: 118– 124, 2012.
[35] E. Meyer, "Untersuchungen über Härteprüfung und Härte Brinell Methoden," *Zeitschrift Des Vereines Deutscher Ingenieure*, 52: 645-654, 740-758, 835-844, 1908.
[36] K. Sangwal. On the reverse indentation size effect and microhardness measurement of solids. *Materials Chemistry and Physics*, 63: 145–152, 2000.
[37] J. Gong, X. Pan, H. Miao, Z. Zhao. Effect of metallic binder content on the microhardness of TiCN-based cermets. *Materials Science and Engineering*, A359: 391-395, 2003.
[38] G. N. Babini, A. Bellosi, C. Galassi. Characterization of hot-pressed silicon nitride-based materials by microhardness measurements. *Journal of Materials Science*, 22: 1687-1693, 1987.
[39] S. J. Bull, T. F. Page and E. H. Yoffe. An explanation of the indentation size effect in ceramics, *Philosophical Magazine Letters*, 59(6): 281-288, 1989.
[40] M. Gee, K. Mingard, B. Roebuck. Application of EBSD to the evaluation of plastic deformation in the mechanical testing of WC/Co hardmetal. *International Journal of Refractory Metals & Hard Materials*, 27: 300–312, 2009.
[41] J. D. Carroll, W. Abuzaid, J. Lambros, H. Sehitoglu. High resolution digital image correlation measurements of strain accumulation in fatigue crack growth. *International Journal of Fatigue*, 57: 140–150, 2013.